GEOPHYSICS, VOL. 71, NO. 3 (MAY-JUNE 2006); P. V51–V60, 12 FIGS., 1 TABLE.
10.1190/1.2192912

Inverse *Q*-filter for seismic resolution enhancement

Yanghua Wang[1]

ABSTRACT

A principal limitation on seismic resolution is the earth attenuation, or *Q*-effect, including the energy dissipation of high-frequency wave components and the velocity dispersion that distorts seismic wavelets. An inverse *Q*-filtering procedure attempts to remove the *Q*-effect to produce high-resolution seismic data, but some existing methods either reduce the S/N ratio, which limits spatial resolution, or generate an illusory high-resolution wavelet that contains no more subsurface information than the original low-resolution data. In this paper, seismic inverse *Q*-filtering is implemented in a stabilized manner to produce high-quality data in terms of resolution and S/N ratio. Stabilization is applied to only the amplitude compensation operator of a full inverse *Q*-filter because its phase operator is unconditionally stable, but the scheme neither amplifies nor suppresses high frequencies at late times where the data contain mostly ambient noise. The latter property makes the process invertible, differentiating from some conventional stabilized inverse schemes that tend to suppress high frequencies at late times. The stabilized inverse *Q*-filter works for a general earth *Q*-model, variable with depth or traveltime, and is more accurate than a layered approach, which involves an approximation to the amplitude operator. Because the earth *Q*-model can now be defined accurately, instead of a constant-*Q* layered structure, the accuracy of the inverse *Q*-filter is much higher than for a layered approach, even when implemented in the Gabor transform domain. For the stabilization factor, an empirical relation is proposed to link it to a user-specified gain limit, as in an explicit gain-controlling scheme. Synthetic and real data examples demonstrate that the stabilized inverse *Q*-filter corrects the wavelet distortion in terms of shape and timing, compensates for energy loss without boosting ambient noise, and produces desirable seismic images with high resolution and high S/N ratio.

INTRODUCTION

High-resolution seismic data are needed for detailed descriptions of oil and gas reservoirs; for determination of spatial heterogeneities such as the spatial variation of porosity, gas content, or pore pressure; and for monitoring temporal changes within a reservoir that result from production. While the development of new methods for high-resolution seismic data acquisition are important, maximum immediate benefit can be obtained by applying methods that can improve the resolution of existing seismic data sets and that can be used with new data sets acquired with existing systems. This paper discusses one such resolution-enhancement technique, the inverse *Q*-filter. Anelasticity and inhomogeneity in the subsurface dissipate high-frequency seismic energy, which decreases seismic amplitudes; they also cause velocity dispersion, thus modifying, delaying, and stretching the seismic wavelet (Kolsky, 1956; Mason, 1958; Futterman, 1962; Trorey, 1962; Strick, 1967; Kjartansson, 1979; Ben-Menahem and Singh, 1981). The energy dissipation and velocity dispersion of the seismic wave require suitable treatment for higher-resolution subsurface reflectivity imaging. This treatment is generally referred to as inverse *Q*-filtering.

When the *Q* of a medium is constant with respect to depth or traveltime, a phase-only inverse *Q*-filter for eliminating velocity dispersion can be implemented efficiently as a Stolt frequency wavenumber migration (Hargreaves and Calvert, 1991). If the subsurface is in a layered *Q*-structure, phase-only inverse *Q*-filtering may be implemented in a layered fashion; within each layer, it is a constant-*Q*, phase-only inverse filter (Bano, 1996). These phase-only inverse *Q*-filters correcting the phase distortion from velocity dispersion are unconditionally stable (Robinson, 1979, 1982; Bickel and Natarajan, 1985) but neglect the amplitude effect from energy dissipation.

Full inverse *Q*-filtering that performs amplitude compensation and phase correction simultaneously can have instability problems and can result in undesirable artifacts in the seismic data. A stabi-

Manuscript received by the Editor September 3, 2003; revised manuscript received September 18, 2005; published online May 24, 2006; corrected version published online June 2, 2006.
[1]Imperial College London, Centre for Reservoir Geophysics, Department of Earth Science and Engineering, London SW7 2BP, United Kingdom. E-mail: yanghua.wang@imperial.ac.uk.

lized method proposed by Wang (2002) can recover all frequency components that in principle are recoverable and can intelligently limit the compensation of a given high-frequency wave component when its amplitude has been attenuated to a level below the ambient noise. Thus, it does not boost ambient noise. This feature is significant because seismic resolution is not only a function of the frequency bandwidth but is also a function of the S/N ratio. A formula for measuring the change in seismic resolution can be found in Wang (2003).

Wang's (2002) full inverse Q-filtering method is implemented as a series of constant-Q inverse filters, corresponding to a stack of constant-Q layers. Within a constant-Q layer, the 2D amplitude compensation operator is approximated optimally as the product of two 1D functions depending on traveltime and frequency, respectively. By doing so, inverse Q-filtering can be implemented in the Fourier domain akin to the phase-only inverse Q-filter mentioned above, which affords efficiency but introduces approximations.

One line of research and development in inverse Q-filtering evolves from constant Q and phase only, layered Q and phase only, layered Q and full inverse Q-filtering, and finally an algorithm of full inverse Q-filtering for a continuous variable Q-model, such as the one presented in this paper. This algorithm is an extension of the layered algorithm presented in Wang (2002) with the following differences.

- The earth Q-model can vary continuously along the subsurface depth or two-way traveltime, while the layered approach needs to approximate the Q-model using constant-Q layers. The latter also involves approximations to the amplitude compensation operator.
- An inverse Q-filter neither suppresses nor amplifies the data components with high frequencies at late times. In real data processing, we often need to redo the inverse Q-filtering with updated Q-function at a later stage. If a data component has been suppressed by inverse Q-filtering, it cannot be recovered afterward.
- Stabilization is applied only to the amplitude compensation operator in full inverse Q-filtering, as its phase correction operator is unconditionally stable. Therefore, the phase component of a full inverse Q-filter is accurate without any damping effect of the stabilization.

To improve efficiency, an alternative but approximate implementation is presented in conjunction with the Gabor transform. The Gabor transform decomposes a time-domain seismic trace by performing localized Fourier transforms successively for a suite of window positions down the seismic trace, generating the time-variant Gabor spectrum (Gabor, 1946; Bastiaans, 1980; Feichtinger and Strohmer, 1998). Inverse Q-filtering can be achieved by modifying the time-frequency-domain Gabor spectrum before trace reconstruction with an inverse Gabor transform.

Theoretically, the stabilization factor should be linked physically to the S/N ratio of the seismic data. Without quantitative prior knowledge of the S/N ratio, I attempt in this paper to establish an empirical relationship between the stabilization factor and a specified gain limit, as in an explicit gain-controlling scheme.

THE INVERSE Q-FILTERING ALGORITHM

Proper inverse Q-filtering is a prerequisite for true-amplitude recovery for the purpose of, for example, amplitude inversion and subsequent reservoir characterization. Also, by correcting the phase distortion, seismic data with enhanced resolution provide correct timings for lithological identification and well ties. To achieve these benefits, stabilized inverse Q-filters are required to produce optimal resultant data quality in terms of both resolution and S/N ratio, as some existing methods either reduce the S/N ratio, which limits spatial resolution, or generate an illusory high-resolution wavelet that contains no more subsurface information than did the original low-resolution starting point. This section describes such a stabilized inverse Q-filtering algorithm for an earth model with a continuous variable Q-function.

Stabilized algorithm

For forward wave propagation, a plane wave $U(x,\omega)$ with travel distance Δx is given by

$$U(x+\Delta x,\omega) = U(x,\omega)\exp[-ik(\omega)\Delta x], \tag{1}$$

where i is the imaginary unit, ω is the angular frequency, and $k(\omega)$ is the wavenumber. The earth Q-effect may be represented with a complex wavenumber

$$k(\omega) = \left(1-\frac{i}{2Q_r}\right)\frac{\omega}{v_r}\left(\frac{\omega}{\omega_h}\right)^{-\gamma}, \tag{2}$$

where Q_r and v_r are the Q-value and the phase velocity at an arbitrary reference frequency; $\gamma = (1/\pi)Q_r^{-1}$, following Kolsky (1953) and Kjartansson (1979); and ω_h is a tuning parameter related to the highest possible frequency of the seismic band (Wang and Guo, 2004a). Note that only positive frequencies are considered in equation 2.

An inverse Q-filter is then given by

$$U(x+\Delta x,\omega) = U(x,\omega)\exp[ik(\omega)\Delta x]. \tag{3}$$

Substituting the complex-valued wavenumber $k(\omega)$ into equation 3 and replacing the distance increment Δx by traveltime increment $\Delta\tau$, we obtain

$$U(\tau+\Delta\tau,\omega) = U(\tau,\omega)\exp\left[\left(\frac{\omega}{\omega_h}\right)^{-\gamma}\frac{\omega\Delta\tau}{2Q_r}\right] \times \exp\left[i\left(\frac{\omega}{\omega_h}\right)^{-\gamma}\omega\Delta\tau\right]. \tag{4}$$

This equation is the basis for an inverse Q-filtering algorithm in which the two exponential operators compensate for the amplitude effect (i.e., the energy absorption) and the phase effect (i.e., the velocity dispersion), respectively.

Considering the earth Q-model as a 1D function $Q(\tau)$ varying with traveltime τ and performing wavefield downward continuation using equation 4 from the surface $\tau_0 = 0$ to the depth-time level τ, we can present the wavefield $U(\tau,\omega)$ as

$$U(\tau,\omega) = U(0,\omega)\exp\left[\int_0^\tau\left(\frac{\omega}{\omega_h}\right)^{-\gamma(\tau')}\frac{\omega}{2Q(\tau')}d\tau'\right] \times \exp\left[i\int_0^\tau\left(\frac{\omega}{\omega_h}\right)^{-\gamma(\tau')}\omega d\tau'\right], \tag{5}$$

where $\gamma(\tau) = (1/\pi)Q^{-1}(\tau)$. The amplitude operator, as shown in equation 5, is an exponential function of frequency and traveltime; a full inverse *Q*-filter including amplitude compensation will cause instability and will generate undesirable artifacts in the seismic data (Wang, 2002). Therefore, stability is the major concern in any scheme for inverse *Q*-filtering.

To stabilize the implementation, let us represent equation 5 as

$$\beta(\tau,\omega)U(\tau,\omega) = U(0,\omega)\exp\left[i\int_0^\tau \left(\frac{\omega}{\omega_h}\right)^{-\gamma(\tau')} \omega d\tau' \right], \tag{6}$$

where

$$\beta(\tau,\omega) = \exp\left[-\int_0^\tau \left(\frac{\omega}{\omega_h}\right)^{-\gamma(\tau')} \frac{\omega}{2Q(\tau')} d\tau' \right]. \tag{7}$$

We then solve equation 6 as an inverse problem with stabilization, producing the following stabilized formula:

$$U(\tau,\omega) = U(0,\omega)\Lambda(\tau,\omega)\exp\left[i\int_0^\tau \left(\frac{\omega}{\omega_h}\right)^{-\gamma(\tau')} \omega d\tau' \right], \tag{8}$$

where

$$\Lambda(\tau,\omega) = \frac{\beta(\tau,\omega) + \sigma^2}{\beta^2(\tau,\omega) + \sigma^2} \tag{9}$$

and σ^2 is the stabilization factor.

Performing equation 8 for all different frequencies and then summing these plane waves (i.e., the imaging condition), we obtain a time-domain seismic sample:

$$u(\tau) = \frac{1}{\pi}\int_0^\infty U(0,\omega)\Lambda(\tau,\omega) \times \exp\left[i\int_0^\tau \left(\frac{\omega}{\omega_h}\right)^{-\gamma(\tau')} \omega d\tau' \right] d\omega. \tag{10}$$

This is the expression of stabilized full inverse *Q*-filtering.

Physical understanding of stabilization

Equation 10 must be performed successively at each time sample τ and may be discretized as

$$\begin{bmatrix} u_0 \\ u_1 \\ \vdots \\ u_M \end{bmatrix} = \begin{bmatrix} a_{0,0} & a_{0,1} & \cdots & a_{0,N} \\ a_{1,0} & a_{1,1} & \cdots & a_{1,N} \\ \vdots & \vdots & & \vdots \\ a_{M,0} & a_{M,1} & \cdots & a_{M,N} \end{bmatrix} \begin{bmatrix} U_0 \\ U_1 \\ \vdots \\ U_N \end{bmatrix}, \tag{11}$$

where $\{u_i \equiv u(\tau_i)\}$ is the time-domain output data vector, $\{U_j \equiv U(\omega_j)\}$ is the frequency-domain input data vector, and $\{a_{i,j}\}$ is the inverse *Q*-filter ($M \times N$) with an element defined as

$$a_{i,j} = \frac{1}{N}\Lambda(\tau_i,\omega_j)\exp\left[i\int_0^{\tau_i} \left(\frac{\omega_j}{\omega_h}\right)^{-\gamma(\tau')} \omega_j d\tau' \right]. \tag{12}$$

To understand stabilization physically, we rewrite equation 11 as

$$\begin{bmatrix} u_0 \\ u_1 \\ \vdots \\ u_M \end{bmatrix} = \sum_\omega U(\omega) \begin{bmatrix} a_0 \\ a_1 \\ \vdots \\ a_M \end{bmatrix}(\omega). \tag{13}$$

That is, the inverse *Q*-filtered wavefield $\{u(\tau)\}$ in the time domain is a weighted superposition of all plane waves $\{U(\omega)\}$. The weighting coefficient series $\{a_i\}$ are time variant, and they act as a nonstationary filter applied to $U(\omega)$.

The weighting coefficients, in general, are an exponential function of time but are modified for stabilization. Expression 13 also offers an intuitive understanding about stabilization. Considering forward wave propagation, when a plane-wave component travels beyond a certain time, its amplitude is attenuated to a level below the ambient noise; accordingly, inverse *Q*-filtering limits the attempt to compensate for it by modifying, the weighting coefficient series. Thus, this series is also frequency dependent.

Stabilization only to amplitude component

Conventionally, one takes the following complex function

$$f(\tau,\omega) = \exp\left[-\int_0^\tau \left(\frac{1}{2Q(\tau')} + i\right)\left(\frac{\omega}{\omega_h}\right)^{-\gamma(\tau')} \omega d\tau' \right] \tag{14}$$

into the stabilization process, as in Wang (2002) and in Irving and Knight (2003). The complex function $f(\tau,\omega)$ in expression 14 consists of full *Q*-effects, including amplitude attenuation and phase distortion. However, because only the inverse of the real part of $f(\tau,\omega)$ is unstable, I propose in equation 9 to stabilize only the inverse of the real exponential function $\beta(\tau,\omega)$ of equation 7. By doing so, we accurately correct the phase.

Stabilization without high-$\omega\tau$ suppression

In the stabilization formula 9, the stabilization factor σ^2 is added to the numerator. The presence of σ^2 in the numerator means that this stabilization scheme does not include the high-$\omega\tau$ suppression (Figure 1a). Without high-$\omega\tau$ suppression in stabilization, we can accurately remove the amplitude compensation previously added to the seismic data by inverse *Q*-filtering, if we need to do so. The associated operator for removal is the inverse of the compensation

operator, $\tilde{\beta}(\tau,\omega) = \Lambda^{-1}(\tau,\omega)$. In practice, we often require that processing operations be removable so that we can easily optimize the processing parameters later.

Conventionally, a stabilization formula is given by

$$\Lambda_c(\tau,\omega) = \frac{\beta(\tau,\omega)}{\beta^2(\tau,\omega) + \sigma^2}, \tag{15}$$

which is used extensively in the inverse problem (Berkhout, 1982). In the context of inverse Q-filtering, a justification may be given as follows: When a plane wave with frequency ω propagates through a subsurface medium after a certain traveltime τ, its energy is absorbed completely. Using this stabilized operator, inverse filtering with an accurate Q-model suppresses the high-frequency noise in the seismic data. Thus, equation 15 may be referred to as a stabilization scheme with high-$\omega\tau$ suppression.

To compare these two schemes, I plot the amplitude coefficients as a function of the product of ω and τ (Figure 1). For the first stabilization scheme without high-$\omega\tau$ suppression, high-frequency data components are not boosted by the inverse Q-filter and are not altered in subsequent forward Q-modeling. For the second scheme with high-$\omega\tau$ suppression, the data are filtered simultaneously with a time-variant low-pass filter, designed naturally according to the earth Q-model. But this second stabilized operator is not invertible. I propose to define the associated amplitude attenuation operator by

$$\tilde{\beta}_c(\tau,\omega) = \frac{\Lambda_c(\tau,\omega)}{\Lambda_c^2(\tau,\omega) + |\sigma|}, \tag{16}$$

where the stabilization factor is $|\sigma|$ instead of σ^2. By doing so, as shown in Figure 1b, the amplitudes within the range $[0, 300\pi]$ can be recovered accurately. At $\omega\tau = 300\pi$, $\Lambda(\tau,\omega) = 1$. At about $\omega\tau = 370\pi$, a peak indicates the curve (the dotted line) beyond this point has been damped and otherwise would be increasing exponentially. If σ^2 were used in equation 16, the amplitudes within the range $[150\pi, 300\pi]$ would not have been recovered accurately and, instead, would have been damped toward zero. Note that both $\Lambda_c(\tau,\omega)$ and $|\sigma|$ in equation 16 are dimensionless.

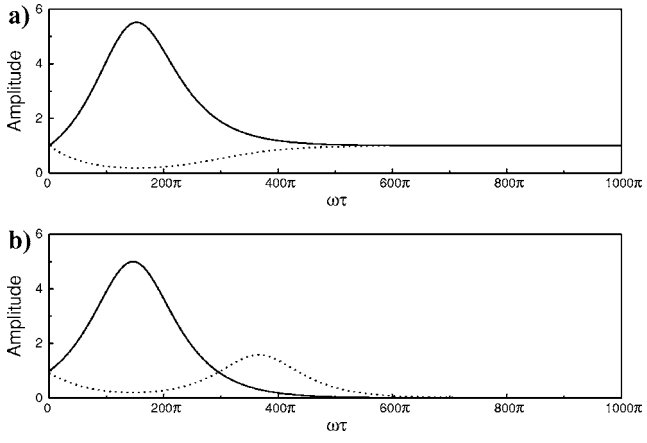

Figure 1. Two stabilization schemes (a) without and (b) with high-$\omega\tau$ suppression. The solid lines are the amplitude-compensation coefficients of an inverse Q-filter. The dashed lines are the associated amplitude coefficients needed for compensation removal.

IMPLEMENTATION WITH GABOR TRANSFORM

As mentioned before, full inverse Q-filtering (expression 10) with time-dependent Q-function must be performed successively for each time sample. To improve efficiency, this section describes an implementation in the Gabor transform domain.

We start the derivation with equation 8. Assuming a medium with $Q^{-1} = 0$, the wavefield recorded at depth-time level τ can be obtained from equation 8 as

$$\tilde{U}(\tau,\omega) = U(0,\omega)\exp[i\omega\tau]. \tag{17}$$

Using $\tilde{U}(\tau,\omega)$, equation 8 becomes

$$U(\tau,\omega) = \tilde{U}(\tau,\omega)\Lambda(\tau,\omega) \times \exp\left[i\int_0^\tau \left(\left(\frac{\omega}{\omega_h} \right)^{-\gamma(\tau')} - 1 \right) \omega d\tau' \right]. \tag{18}$$

Both $U(\tau,\omega)$ and $\tilde{U}(\tau,\omega)$ are the wavefield recorded at the depth-time level τ, but the latter has no inverse Q-filtering.

Equation 18 is the central equation for the Gabor transform-based inverse Q-filtering algorithm. I now describe, given a time-domain seismic trace $u(t)$, how to compute $\tilde{U}(\tau,\omega)$ and, after inverse Q-filtering, how to reconstruct $u(t)$ from $U(\tau,\omega)$ by using the Gabor transform.

The forward Gabor transform is defined as

$$\tilde{U}(\tau,\omega) = \int_{-\infty}^{\infty} u(t)w(t-\tau)\exp[-i\omega t]dt, \tag{19}$$

where $w(t)$ is the Gabor analysis window and τ is the location of the window center. Defining a Gabor slice as

$$\tilde{u}(\tau,t) = u(t)w(t-\tau), \tag{20}$$

we see the Gabor transform of $u(t)$ is the Fourier transform of the Gabor slices for all possible τ locations with respect to time t:

$$\tilde{U}(\tau,\omega) = \mathcal{F}\{\tilde{u}(\tau,t)\}. \tag{21}$$

The Gabor analysis window is a Gaussian window:

$$w(t) = \begin{cases} \dfrac{2}{T\sqrt{\pi}} \exp\left[-4\left(\dfrac{t}{T} \right)^2 \right], & \text{for } -T \le t \le T, \\ 0, & \text{otherwise}, \end{cases} \tag{22}$$

where T is referred to as the (half) width of the window. The Hamming window can also be used as the Gabor analysis window, but a simple boxcar function without tapering cannot be used because when a segment of digital signal is transformed into the frequency domain, it may have a side-lobe effect in the spectrum. Such spectral errors are severely amplified by inverse Q-filtering.

Applying inverse Q-filtering to $\tilde{U}(\tau,\omega)$ using equation 18, produces a modified Gabor transform spectrum $U(\tau,\omega)$. In the layered implementation (Wang, 2002), the imaging condition (summing over the frequency axis) was applied to $U(\tau,\omega)$ to produce the final seismic trace in the time domain. In the Gabor transform method, after inverse Q-filtering on the wavefield, an inverse Gabor transform is used to reproduce the time-domain trace.

The inverse Gabor transform that recovers signal $u(t)$ from the Gabor transform spectrum $U(\tau,\omega)$ is defined as

$$u(t) = h(t)\int_{-\infty}^{\infty}\int_{-\infty}^{\infty} U(\tau,\omega)\exp[i\omega t]d\omega d\tau, \qquad (23)$$

where $h(t)$ is the Gabor synthesis window. It consists of an inverse Fourier transform with respect to the frequency

$$u(\tau,t) = \mathcal{F}^{-1}\{U(\tau,\omega)\}, \qquad (24)$$

which reproduces the Gabor slice and then the data synthesis integral:

$$u(t) = h(t)\int_{-\infty}^{\infty} u(\tau,t)d\tau. \qquad (25)$$

The Gabor synthesis window $h(t)$, which can be derived by substituting equation 20 into equation 25, may be expressed as

$$h(t) = \left[\int_{-\infty}^{\infty} w(t-\tau)d\tau\right]^{-1}. \qquad (26)$$

The synthesis window here is expressed in terms of the Gabor analysis window $w(t)$ to mitigate the potential numerical errors caused by digitization on the Gabor analysis window and the edge effect when moving the analysis window toward the two ends of a seismic trace.

The Gabor transform implementation is still an approximation but should be much more accurate than the layered implementation in Wang (2002). For a window center at the time sample τ, since the inverse Q-filter is calculated using a Q-value at τ, the upper half-window trace segment (time $<\tau$) tends to be overcompensated and the lower half-window trace segment (time $>\tau$) tends to be undercompensated. In the layered implementation, the trace segment within the whole window, corresponding to a layer, is stored as the output. In the Gabor transform implementation, however, an undercompensated half-window segment, and an overcompensated half-window segment of the two neighboring windows, are mixed (i.e., data synthesis integral, equation 25) to generate the final output. This gives greater accuracy and also overcomes the potential artifacts in the inverse Q-filtered traces from the discontinuity in the layered Q-model.

Figure 2 compares synthetic seismic traces ($Q = 88$) and the associated Gabor transform spectra before and after inverse Q-filter-ing. The Gabor transform spectra clearly show that frequency content changes with time and changes with/without inverse Q-filter-ing. Figure 3 shows that when a high-frequency plane wave has been attenuated completely from the input seismic data, the stabi-lized inverse Q-filtering procedure automatically limits the attempt to recover it. It also shows that the phase after inverse Q-filtering becomes zero phase within the frequency range $[0,62]$ Hz.

STABILIZATION FACTOR VERSUS GAIN LIMIT

In this section, I attempt to derive an empirical relationship between the stabilization factor σ^2 and a specified gain limit to con-

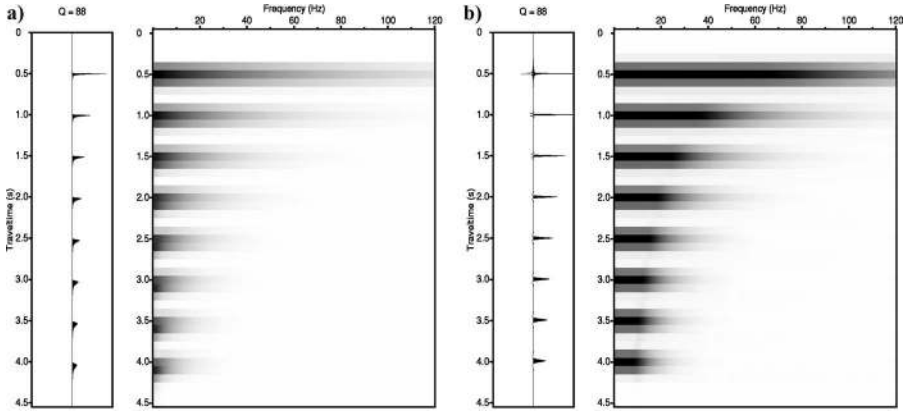

Figure 2. Synthetic seismic traces ($Q = 88$) and their Gabor transform spectra (a) before and (b) after inverse Q-filtering.

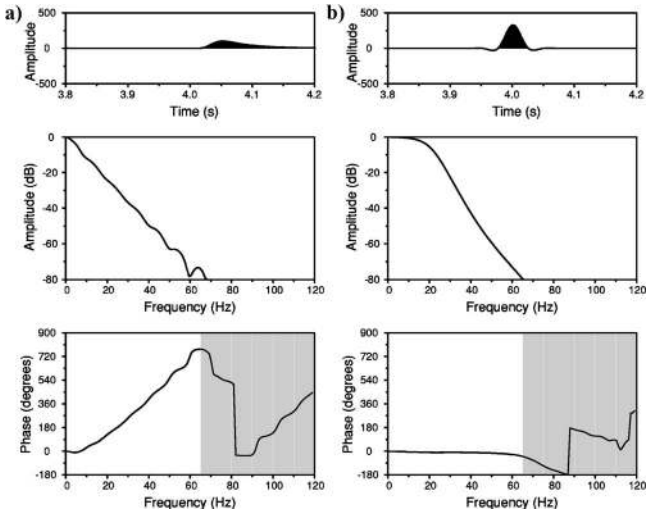

Figure 3. The amplitude and phase spectra of a single wavelet ($Q = 88$, time = 4 s) (a) before and (b) after inverse Q-filtering. If a plane wave with high frequency (≥ 62 Hz) has been attenuated completely from the input seismic data, stabilized inverse Q-filtering automatically limits the attempt to recover it. Within the frequency range $[0,62\,\text{Hz}]$ where amplitude spectra are greater than -80 dB, the phase of the wavelet has been fully recovered by inverse Q-filtering, and the wavelet appears to be zero phased.

trol explicitly the amplitude gain in inverse Q-filtering. The empirical formula is given as

$$\sigma^2 = \exp[-(0.23G_{\lim} + 1.63)] \tag{27}$$

or, equivalently, $G_{\lim} = -7.087 - 4.348 \ln \sigma^2$, where $G_{\lim}$ is the specified gain limit in decibels.

To derive the stabilization factor, let us define a variable $\chi \equiv \omega\tau$ and represent the stabilized amplitude operator (equation 9) as

$$\Lambda(\chi) = \frac{\beta(\chi) + \sigma^2}{\beta^2(\chi) + \sigma^2}. \tag{28}$$

In practice, one may prefer to set a threshold to control the amplitude gain in inverse Q-filtering as

$$\hat{\Lambda}(\chi) = \begin{cases} g(\chi), & \text{for } \chi \le \chi_q, \\ g_{\lim}, & \text{for } \chi > \chi_q, \end{cases} \tag{29}$$

where $g_{\lim} = \exp[G_{\lim}/20]$ and χ_q is the critical point where the gain curve is cut off (Figure 4). Here, assuming a constant Q along a seismic trace, $\beta(\chi)$ and $g(\chi)$ functions in equations 28 and 29 are given as $\beta(\chi) = \exp[-\chi/(2Q)]$ and $g(\chi) = \exp[\chi/(2Q)]$, respectively.

To estimate σ^2 empirically, let us now set up a criterion: The integrals up to the crosspoint χ_a (as shown in Figure 4) of two individual gain curves are equivalent. That is, we estimate σ^2 by solving the following two equations simultaneously:

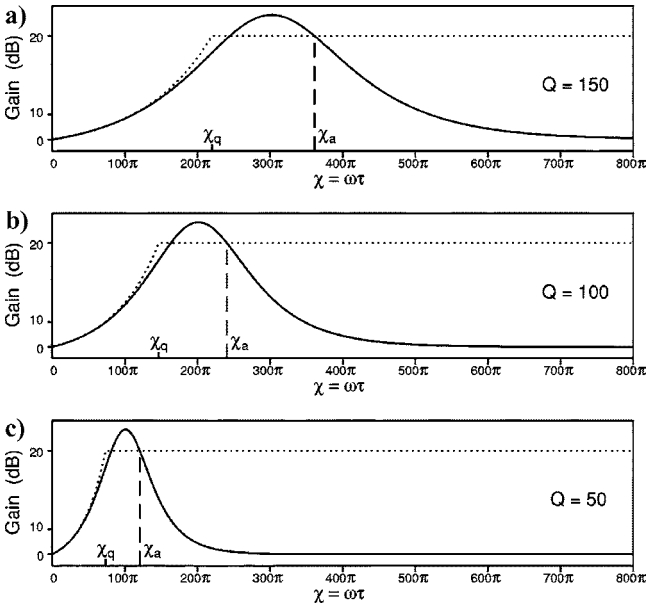

Figure 4. Comparison of the gain curves of inverse Q-filtering with an explicit gain-controlling scheme (dotted lines) and the stabilized scheme (solid lines). The horizontal coordinate is $\chi \equiv \omega\tau$, where ω and τ are frequency and traveltime, respectively. The corner position χ_q corresponds to the cutoff gain limit ($G_{\lim} = 20$ dB, for example), whereas χ_a is a point where the accumulations of two individual gain curves are equivalent.

$$\left.\begin{aligned} \Lambda(\chi_a) &= \hat{\Lambda}(\chi_a) \\ \int_0^{\chi_a} \Lambda(\xi)d\xi &= \int_0^{\chi_a} \hat{\Lambda}(\xi)d\xi \end{aligned}\right\}. \tag{30}$$

Using stabilization formula 28 and gain-limited formula 29, we have the following expressions:

$$\Lambda(\chi_a) = \frac{\exp\left(-\frac{\chi_a}{2Q}\right) + \sigma^2}{\exp\left(-\frac{\chi_a}{Q}\right) + \sigma^2}, \tag{31a}$$

$$\hat{\Lambda}(\chi_a) = g_{\lim}, \tag{31b}$$

$$\int_0^{\chi_a} \Lambda(\xi)d\xi = \frac{2Q}{\sigma^2}\left[\tan^{-1}\left(\frac{1}{\sigma^2}\right) - \tan^{-1}\left(\frac{\exp\left(-\frac{\chi_a}{2Q}\right)}{\sigma^2}\right) + \frac{\sigma^2}{2}\ln\left(\frac{1 + \sigma^2\exp\left(\frac{\chi_a}{Q}\right)}{1 + \sigma^2}\right)\right], \tag{31c}$$

and

$$\int_0^{\chi_a} \hat{\Lambda}(\xi)d\xi = 2Q\left[\exp\left(\frac{\chi_q}{2Q}\right) - 1\right] + (\chi_a - \chi_q)g_{\lim}. \tag{31d}$$

Substituting expressions 31 into equation system 30, we can solve the stabilization factor σ^2 numerically. Fitting a group of σ^2 for given gain limits between 10 and 100 dB produces the empirical formula 27. For a given gain limit, the σ^2 conversion is independent of Q-values.

Figure 4 displays the amplitude compensation curves for various Q-values of the stabilization scheme using σ^2 (solid lines) and the explicit gain-controlling scheme with $G_{\lim} = 20$ dB (dotted lines). A gain-limited scheme attempts to boost amplitude all the way down to the end of the seismic trace, though the gain is controlled by $G_{\lim}$. However, a plane wave with specific frequency ω is attenuated completely after it propagates beyond a certain traveltime τ and has left no information in the seismic record. The conventional gain-limited inverse Q-filtering scheme will boost ambient noise. The stabilized inverse Q-filter recognizes this fact by reducing the gain coefficient gradually and neatly.

SYNTHETIC EXAMPLES

Figure 5a displays five synthetic traces with different Q-values ($Q = 400$, 200, 100, 50, and 25) constant with depth in each case. The basic downward-continuation scheme (equation 5) is applied to this group of noise-free traces. The result (Figure 5b) clearly reveals the numerical instability of inverse Q-filtering. For traces with $Q = 400$ and 200, the process restores the Ricker wavelet

with correct phase and amplitude. However, there are strong artifacts as the Q-value decreases and the imaging time increases, even though the input signal is noise free. The appearance of noise in the output signal is a consequence of the basic inverse Q-filter procedure: A plane wave is attenuated gradually, and beyond a certain distance the signal is below the ambient noise level; but the amplification required to recover the signal amplifies the ambient noise. In the data-noise-free case here, the background noise is the numerical errors from finite machine precision. The cause of strong artifacts is referred to as the numerical instability of the inverse Q-filter.

Figures 5c and 5d display the results of the gain-limited and stabilized inverse Q-filtering schemes, respectively. From these two figures, we can make two observations. First, both methods overcome the instability problem in inverse Q-filtering and successfully suppress the numerical artifact appearing in Figure 5b. Second, stabilized inverse Q-filtering produces a superior result, as the amplitudes of more high-frequency components have been compensated. It has recovered all frequency components that are, in principle, recoverable and has intelligently limited the attempt to amplify ambient noise. The difference between these two results seems marginal when accounting for all possible approximations involved in the seismic data processing flow. However, if these two algorithms are applied to a noisy data set, we see a significant difference between them.

I now apply the gain-limited and stabilized schemes to a group of traces with added weak random noise (Figure 6a). The added noise is so weak that it is hardly visible on the plot. Over the five synthetic traces, the ratio of the maximum noise amplitude and the maximum signal amplitude is only 2%. Even with such weak noise in the input, the gain-limited inverse Q-filter has boosted the noise (Figure 6b). The smaller the Q-value, the stronger the noise is boosted by inverse Q-filtering. The gain limit here is set at $\omega_q = 2Q/\tau$ (Wang, 2002), which is equivalent to $G_{\text{lim}} = 8.69$ dB.

To suppress the noise in Figure 6b, a band-pass filter to cut off the high-frequency noise at late time must be applied (Bickel and Natarajan, 1985). Figure 6c is the filtered result of Figure 6b by applying a Butterworth filter with a 65-Hz cutoff frequency. Even doing so, traces with small Q-values still have strong low-frequency noise. Conversely, as shown in Figure 6d, stabilized inverse Q-filtering produces a result with a much higher S/N ratio. Following equation 27, the stabilization factor $\sigma^2 = 2.66\%$ is used in Figure 6d.

Gain limit plus high-cut filter is not equivalent to the stabilized scheme. Figure 7 shows the amplitude operators of the gain-limited (dotted line) and stabilized (solid line) schemes. The gain curve is the compensation coefficients of all frequency components at a specified time sample—in this case, at $\tau = 1$ or 2 s. Summing all weighted frequency components (imaging condition) generates only one sample at time τ. In Figure 6c, however, the high-cut filter is applied to the entire inverse Q-filtered trace (Figure 6b), not to the gain curve, and thus is not equivalent to applying a Butterworth filter to the gain-limited curve in Figure 7.

Certainly, stabilized inverse Q-filtering is noise-level dependent, and the stabilization factor σ^2 needs to be adjusted accordingly. In the discussion here, let us assume that, in practice, the noise level in the input is very weak, as one might have applied some advanced random noise attenuation techniques prior to inverse Q-filtering (Wang, 1999).

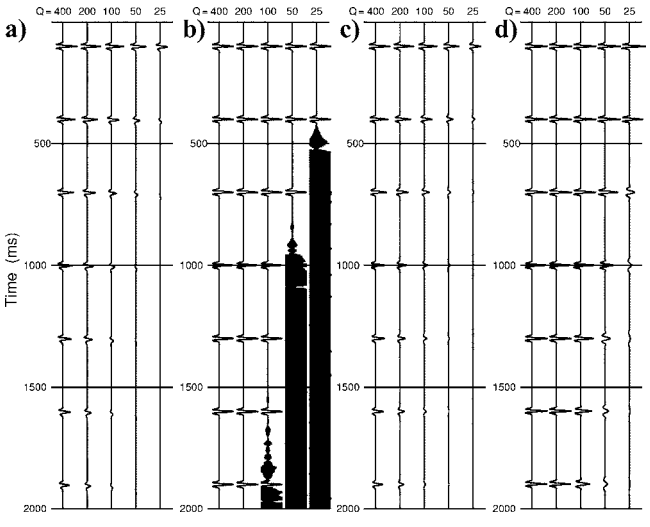

Figure 5. Noise-free synthetic traces and the result of two inverse Q-filtering algorithms. (a) Synthetic seismic traces show the effect of earth Q-filtering with different Q-values. (b) The inverse Q-filtered (compensating for both phase and amplitude) result clearly indicates the numerical instability. (c) The result of gain-limited inverse Q-filtering. (d) The result of a stabilized inverse Q-filtering approach; it has recovered all frequency components that are in principle recoverable and has intelligently limited the attempt to compensate a given high-frequency wave component when its amplitude has been attenuated to a level below the ambient noise level.

REAL DATA EXAMPLES

I now compare the stabilized inverse Q-filter with the following conventional inverse Q-filter (Hale,1981,1982; Varela et al., 1993):

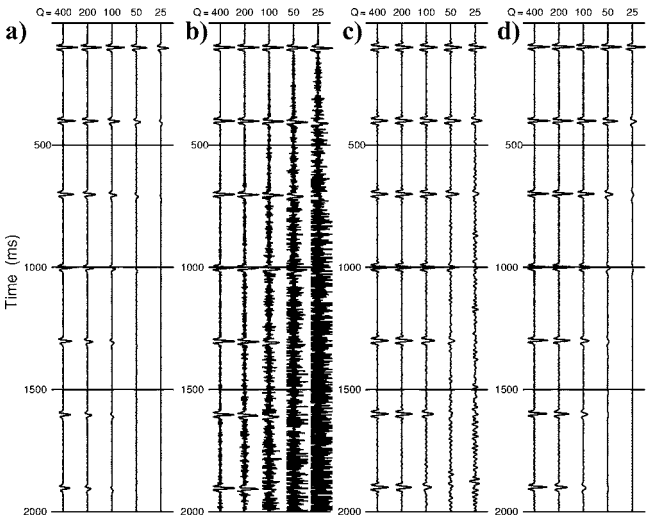

Figure 6. Noise-added synthetic traces and the result of two inverse Q-filtering algorithms. (a) Synthetic seismic traces added with weak random noise (over the five traces, the ratio of the maximum noise amplitude to the maximum signal amplitude is only 2%). (b) Gain-limited inverse Q boosts the noise. (c) The gain-limited result after applying the Butterworth high-cut filter with a 65-Hz cutoff frequency. (d) Stabilized inverse Q-filtering produces a result with a much higher S/N ratio, compared to the gain-limited inverse Q-filtering results in (b) and (c).

$$A(\tau,\omega) = \exp\left[(\omega + i\mathcal{H}\{\omega\})\frac{\tau}{2Q}\right], \qquad (32)$$

where $\mathcal{H}$ is the Hilbert transform. This conventional algorithm is derived straightforwardly from the inverse of the earth Q-filter. To control the enthusiasm of such an inverse Q-process, one often defines a Butterworth spectrum in terms of a high cutoff frequency and a slope. In practice, one often designs a series of inverse Q-filters for given times with given Q-values and associated Butterworth high-cut characteristics and then applies these filters to the seismic trace in a linear piecewise fashion to simulate continuously varying Q-compensation.

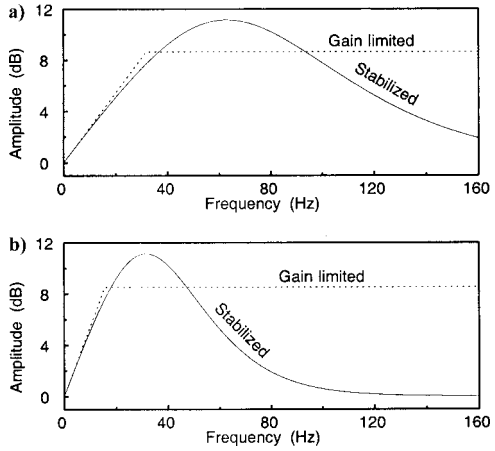

Figure 7. The amplitude operators of gain-limited (dotted line) and stabilized (solid line) inverse Q-filtering schemes at sample time τ of (a) 1 and (b) 2 s for $Q = 100$.

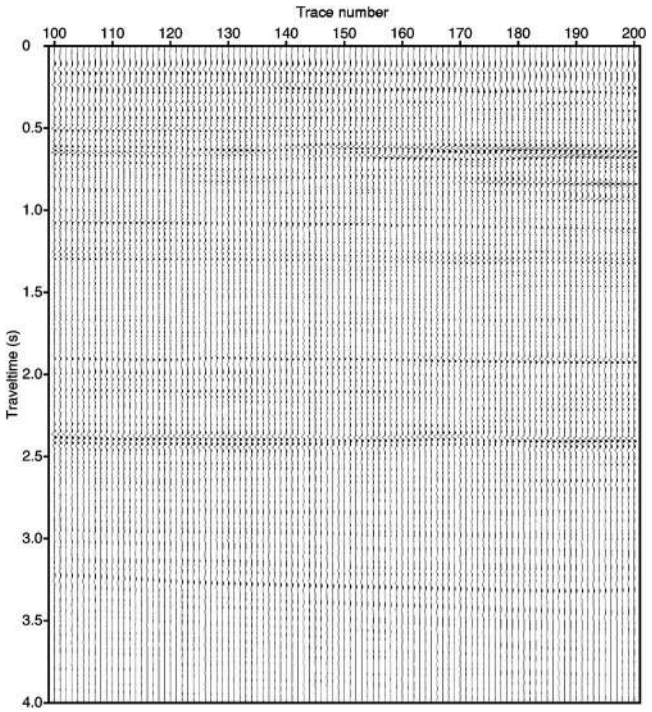

Figure 8. A seismic section with a very high S/N ratio. Its inverse Q-filtering results are shown in Figures 9 and 10.

Figure 8 shows a line of marine seismic reflection data with a very high S/N ratio, compared to a land seismic data section. The results of conventional and stabilized inverse Q-filtering are shown in Figures 9 and 10, respectively. Without knowledge of the Q-value, $Q = 100$ is set in the test. Such a modest Q-value is adopted here mainly to minimize the noise after conventional inverse Q-filtering. Conventional inverse Q-filtering boosts ambient noise and degrades the S/N ratio of the output section. In comparison, the stable inverse Q-filtering method produces a superior result by increasing the frequency bandwidth without degrading the S/N ratio, thereby improving the interpretability of the seismic section.

A fundamental difference between the conventional and the stabilized inverse Q-filtering procedures is that the conventional method applies a low-pass filter as a damage controller to suppress the noise caused by inverse Q-filtering while the stabilized approach attempts to find a stable operator for inverse Q-filtering. In Figure 9, a Butterworth filter is designed with a high-cut frequency of 65 Hz and a slope of 60 dB per octave. In Figure 10, a stabilization factor $\sigma^2 = 0.5\%$ is used for such a data set with high S/N ratio. It is equivalent to $G_{\text{lim}} = 15.9$ dB.

Finally, Figures 11 and 12 show another example of stabilized inverse Q-filtering on a land seismic data set, which usually has a low S/N ratio. In this example, I estimate Q-values from the stack section and then use them for inverse Q-filtering. The Q-analysis method described in Wang (2004b) consists of four steps:

1) Measure time–frequency-dependent attenuation from seismic data.
2) Generate a compensation curve based on the attenuation.
3) Fit the compensation curve with a function in the least-squares sense to invert for the average Q-function.
4) Calculate the interval Q-values.

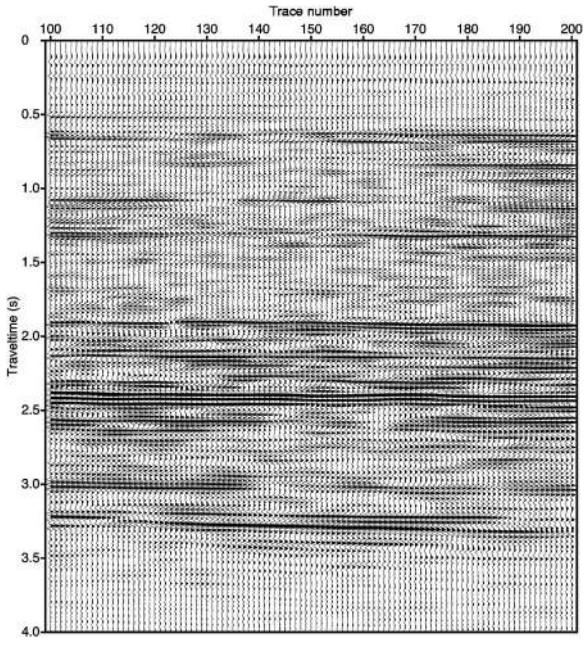

Figure 9. A seismic section after conventional inverse Q-filtering ($Q = 100$), in which a Butterworth filter is designed with a 65-Hz high-cut frequency and a 60-dB/octave slope. Conventional inverse Q-filtering boosts the ambient noise and degrades the S/N ratio of the output section.

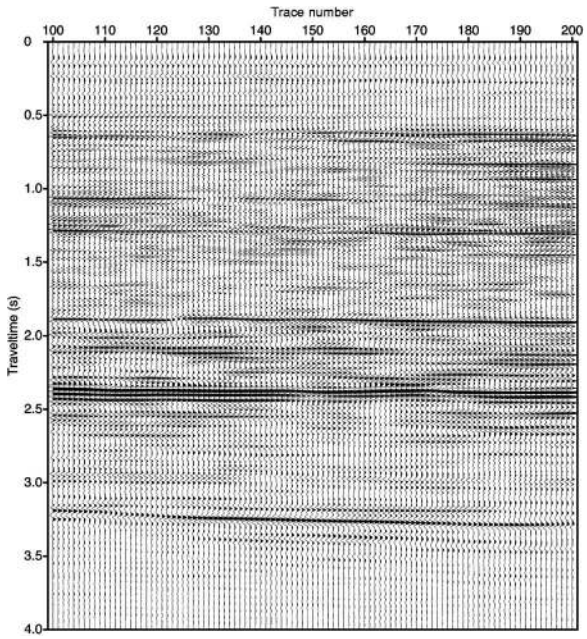

Figure 10. Seismic section after stabilized inverse *Q*-filtering ($Q = 100$, $\sigma^2 = 0.5\%$). The stabilized scheme improves the interpretability of the seismic section by increasing the frequency bandwidth without degrading the S/N ratio.

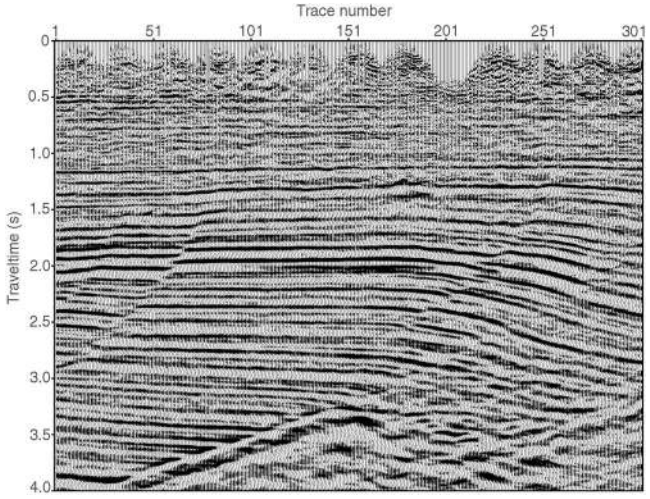

Figure 11. A land seismic stack section for inverse *Q*-filtering. In this plot, a time-squared gain recovery is applied to boost the weak amplitudes for an easy visual comparison to the inverse *Q*-filtered result shown in Figure 12.

The interval *Q*-values obtained from such a *Q*-analysis procedure are listed in Table 1.

Note that in Figure 11 a time-squared gain recovery is applied to boost the weak amplitudes for an easy visual comparison to the inverse *Q*-filtered result shown in Figure 12. Any improvement in continuity of the events in Figure 12 should be reliable because the inverse *Q*-filtering algorithm works trace by trace (i.e., it is not a multichannel process). The example section is selected arbitrarily from a 3D land seismic cube. We would expect that if inverse *Q*-filtering were applied to the whole 3D stack database, it would enhance the 3D migration process, which would benefit from the higher bandwidth. For application in the prestack domain, Wang and Guo (2004b) suggest performing seismic inverse *Q*-filtering and migration simultaneously.

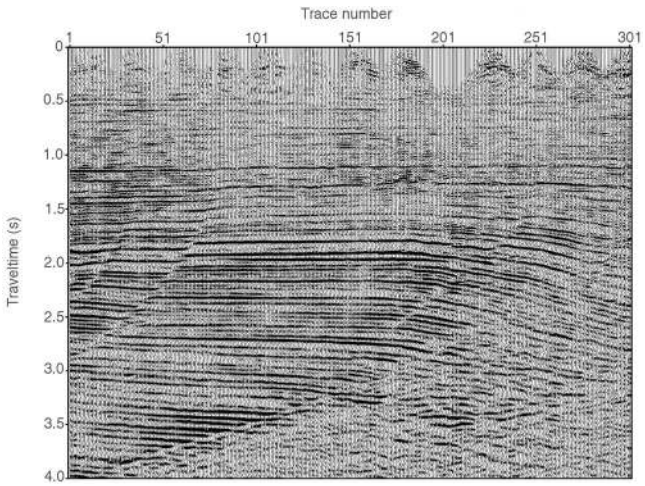

Figure 12. The land seismic section after inverse *Q*-filtering. Any improvement in the continuity of the events should be reliable because the inverse *Q*-filtering algorithm works trace by trace (i.e., is not a multichannel process).

Table 1. The interval *Q*-values obtained from the *Q*-analysis procedure described in Wang (2004).

Time (s)	*Q*
0.1–1	47.5
1–1.5	47.5
1.5–2	65.8
2–2.5	83.0
2.5–3	95.8
3–3.5	108.0
3.5–4	128.0

CONCLUSIONS

The inverse *Q*-filtering algorithm presented in this paper works for a general earth *Q*-model variable with depth or traveltime. It is more accurate than a layered approach proposed previously because (a) the earth *Q*-model can be more accurately defined, instead of constant *Q*-layered structure, and (b) the implementation is more accurate, as the exact solution does not involve the amplitude operator approximation. Even if using Gabor transform implementation, the accuracy is much higher than the layered implementation.

In the full inverse *Q*-filter that includes phase and amplitude operators, we apply stabilization to the amplitude component only, recognizing the phase operator in inverse *Q*-filtering is unconditionally stable. By doing so, we have an exact solution for the phase correction. In the stabilization, the amplitude compensation gain curve approaches 0 dB for high frequencies — that is, it leaves the high-frequency components untouched, neither amplify-

ing nor suppressing. This property is different from a conventional stabilized inverse problem, which tends to suppress high frequencies. In this paper I have also derived an empirical relationship that links the stabilization factor to a specified gain limit given in practice.

REFERENCES

Bano, M., 1996, *Q*-phase compensation of seismic records in the frequency domain: Bulletin of the Seismological Society of America, **86**, 1179–1186.

Bastiaans, M. J., 1980, Gabor's expansion of a signal into Gaussian elementary signals: Proceedings of IEEE, **68**, 538–539.

Ben-Menahem, A., and S. J. Singh, 1981, Seismic waves and sources: Springer-Verlag New York.

Berkhout, A. J., 1982, Seismic migration: Imaging of acoustic energy by wavefield extrapolation: Elsevier Science Publ. Co., Inc..

Bickel, S. H., and R. R. Natarajan, 1985, Plane-wave *Q* deconvolution: Geophysics, **50**, 1426–1439.

Feichtinger, H. G., and T. Strohmer, 1998, Gabor analysis and algorithms — Theory and applications: Birkhäuser-Verlag.

Futterman, W. I., 1962, Dispersive body waves: Journal of Geophysical Research, **67**, 5279–5291.

Gabor, D., 1946, Theory of communication: Journal of the Institute of Electrical Engineers, **93**, 429–457.

Hale, D., 1981, *Q* and adaptive prediction error filters: Stanford Exploration Project Report 28, 209–231.

———, 1982, *Q*-adaptive deconvolution: Stanford Exploration Project Report 30, 133–158.

Hargreaves, N. D., and A. J. Calvert, 1991, Inverse *Q* filtering by Fourier transform: Geophysics, **56**, 519–527.

Irving, J. D., and R. J. Knight, 2003, Removal of wavelet dispersion from GPR data: Geophysics, **68**, 960–970.

Kjartansson, E., 1979, Constant *Q* wave propagation and attenuation: Journal of Geophysical Research, **84**, 4737–4748.

Kolsky, H., 1953, Stress waves in solids: Clarendon Press.

———, 1956, The propagation of stress pulses in viscoelastic solids: Philosophical Magazine, **1**, 693–710.

Mason, W. P., 1958, Physical acoustics and properties of solids: Van Nostrand Reinhold.

Robinson, J. C., 1979, A technique for the continuous representation of dispersion in seismic data: Geophysics, **44**, 1345–1351.

———, 1982, Time-variable dispersion processing through the use of phased sinc functions: Geophysics, **47**, 1106–1110.

Strick, E., 1967, The determination of *Q*, dynamic viscosity and transient creep curves from wave propagation measurements: Geophysical Journal of the Royal Astronomical Society, **13**, 197–218.

Trorey, A. W., 1962, Theoretical seismograms with frequency and depth dependent absorption: Geophysics, **27**, 766–785.

Varela, C. L., A. L. Rosa, and T. J. Ulrych, 1993, Modeling of attenuation and dispersion: Geophysics, **58**, 1167–1173.

Wang, Y., 1999, Random noise attenuation using forward-backward linear prediction: Journal of Seismic Exploration, **8**, 133–142.

———, 2002, A stable and efficient approach to inverse *Q*-filtering: Geophysics, **67**, 657–663.

———, 2003, Quantifying the effectiveness of stabilized inverse *Q*-filtering: Geophysics, **68**, 337–345.

———, 2004, *Q* analysis on reflection seismic data: Geophysical Research Letters, **31**, L17606.

Wang, Y., and J. Guo, 2004a, Modified Kolsky model for seismic attenuation and dispersion: Journal of Geophysical Engineering, **1**, 187–196.

———, 2004b, Seismic migration with inverse *Q*-filtering: Geophysical Research Letters, **31**, L21608.